Feasibility of VERDICT-MRI for non-invasive characterisation of rectal cancer microstructure

Maira Tariq[1], Christopher Liao[2], Elisenda Bonet-Carne[1,3], Andrew A Plumb[2], Manuel Rodriguez-Justo[4], Daniel C Alexander[1], Manish Chand[2], David Atkinson[3], and Eleftheria Panagiotaki [1]

[1]Centre for Medical Image Computing, Department of Computer Science, University College London, London, United Kingdom, [2]University College London Hospital, London, United Kingdom, [3]Centre for Medical Imaging, University College London, London, United Kingdom, [4]Department of Pathology, University College London Hospital, London, United Kingdom

Synopsis

This work evaluates the feasibility of in-vivo microstructure imaging for rectal cancer using the VERDICT MRI framework. We perform a model comparison to find the form of VERDICT that can describe the rich DW-MRI data. Preliminary results from two subjects show promise for non-invasive clinical rectal cancer characterisation. We find that a multi-compartment VERDICT model that explicitly models restriction explains the signal in the rectal tissue better than the conventional cancer models and shows plausible estimates of microstructure in the rectal cancer tissue. Future work will compare these findings with corresponding histology.

INTRODUCTION

Imaging is fundamental to rectal cancer diagnostic and treatment planning. However, there are limitations in the current MRI techniques for rectal cancer staging, predicting response and prognosis[1]. The Vascular, Extracellular, and Restricted Diffusion for Cytometry in Tumours (VERDICT) framework[2] could improve currently used imaging techniques via superior staging, prognostication, and evaluation of treatment response. VERDICT uses a rich in-vivo diffusion-weighted MRI (DW-MRI) acquisition with a computational tissue model to estimate tumour parameters such as cell size, vascular and cellular volumes/density, and perfusion, permitting more precise biological phenotyping. VERDICT has shown promise for clinical differentiation of benign and cancerous tissue[3], as well as characterisation of specific cancer grades[4]. The feasibility of VERDICT modelling in rectal cancer has been shown via a preclinical study[2], demonstrating its use in differentiation of cancer type and response to treatment. Here we explore the translation of VERDICT to clinical rectal cancer imaging, to obtain non-invasive microstructure-specific measures.

METHODS:

MR imaging:

Two male subjects with biopsy-proven rectal cancer were recruited for the study. DW-MRIs were acquired on a 3T-Philips Achieva MRI, using PGSE sequence (EPI read-out) and 1.25x1.25x5mm^3 resolution. The acquisition had multiple b-values and diffusion times, summarised in Figure.1a, to support estimation of various multi-compartment models. A high-resolution T2-weighted MRI was acquired for anatomical reference. Motion correction[5] was applied to account for tissue movement.

Data analysis

To assess which microstructural models best explain the signal in rectal tissue, we compare 13 plausible compartment models listed in Figure.1b. These models are combinations of: sphere (isotropic diffusion restricted with radius R), stick (diffusion restricted to a single direction), ball (isotropic free diffusion) and zeppelin (anisotropic cylindrically symmetric free diffusion), using terminology in[6]. We also include the conventional models: ADC (Ball) and IVIM (BallBall). We do model fitting using the non-linear fitting procedure as used in[3], with data normalised using the b=0 for each echo time, to account for T2 dependence.

A certified board radiologist drew regions-of-interest (ROIs) to include cancerous tissue from the rectal wall, as shown in Figure.2a. We perform model fitting for the ROIs without fixing any of the model parameters. To find the model which best describes the diffusion signal, we do model comparison using the Bayesian Information Criterion (BIC)[7]. To demonstrate microstructure parametric maps over the rectal tissue, we do voxel-wise fitting with one of the best-ranked models. To improve fitting stability for these maps we fix the intrinsic diffusivity to $1.3 \times 10^{-9} m^2/s$, an indicative value from the ROI analysis[8].

RESULTS:

Model comparison

Figures.3&4 show that two- and three-compartment models that include the sphere compartment best fit the data. The simpler ADC and IVIM models fail to capture the signal particularly for higher b-values as expected. Comparison of the fit of the models to the data shows that among two-compartment models, the ZeppelinSphere performs the best, while for three-compartment models the ZeppelinSphereBall and ZeppelinSphereStick perform the best.

To find the simplest model (least number of parameters) that provides the best fit for the data, we rank the models according to BIC, shown in Figure.2b. We see that overall, the two-compartment ZeppelinSphere has the best ranking, with ZeppelinSphereBall a close second.

Parameter maps

We generate parametric maps using the more general three-compartment model ZeppelinSphereBall that was ranked among the best for both datasets across all ROIs. Figure.5 shows these maps, which include the volume fraction of the restriction compartment (f), intrinsic and vascular diffusivity (D_i, D_1), and the estimated cell dimensions (R). The f maps show an elevation of the intracellular volume fraction in the cancer tissue and the high D_1 values indicate vascular component.

DISCUSSION AND CONCLUSION

Early results show promise for non-invasive rectal characterisation using VERDICT MRI. The models with sphere compartments provide the best fit to the data, showing that isotropic restriction is very important to characterise the rectal cancer signal. The preference of the Zeppelin and Stick compartments in model selection suggests the presence of anisotropy in the signal, particularly for subject 1. Histopathological results for these subjects will shed more light on how well these findings correlate to the microstructure.

We observe anisotropy even with data acquired with only three gradient orientations, and anisotropic models are favoured from model selection. Future work will add more directions to explore this directionality and whether it is cellular or vascular. Future work will also investigate more complex models, e.g. accounting for T2 of different compartments.

A limitation is that the data acquired suffers from distortions, due to magnetic susceptibility, which is a key difficulty resulting from imaging structures near to tissue-tissue or tissue-air boundaries. Future imaging protocol will aid reduction of such distortions using methods like in[9].

Acknowledgements

This work is funded by the EPSRC grant EP/N021967/1 (EP). EP/M020533/1 and EP/N018702/1 support DCA.

References

1. Engin, G. & Sharifov, R. Magnetic resonance imaging for diagnosis and neoadjuvant treatment evaluation in locally advanced rectal cancer: A pictorial review. World J. Clin. Oncol. 8, 214–229 (2017).

2. Panagiotaki, E. et al. Noninvasive Quantification of Solid Tumor Microstructure Using VERDICT MRI. Cancer Res. 74, 1902–1912 (2014).

3. Panagiotaki, E. et al. Microstructural Characterization of Normal and Malignant Human Prostate Tissue With Vascular, Extracellular, and Restricted Diffusion for Cytometry in Tumours Magnetic Resonance Imaging. Invest. Radiol. 50, 218–227 (2015).

4. Johnston, E. et al. Short term repeatability of microstructural (VERDICT) MRI vs. ADC in prostate cancer. in ISMRM (2016).

5. Modat, M., Dagga, P., Clarkson, M. J. & Ourselin, S. NiftyReg: (version 1.3). (2010).

6. Panagiotaki, E. et al. Compartment models of the diffusion MR signal in brain white matter: A taxonomy and comparison. NeuroImage 59, 2241–2254 (2012).

7. Schwarz, G. Estimating the Dimension of a Model. Ann. Stat. 6, 461–464 (1978).

8. Li, H., Jiang, X., Xie, J., Gore, J. C. & Xu, J. Impact of transcytolemmal water exchange on estimates of tissue microstructural properties derived from diffusion MRI. Magn. Reson. Med. 77, 2239–2249 (2017).

9. Andersson, J. L. R., Skare, S. & Ashburner, J. How to correct susceptibility distortions in spin-echo echo-planar images: application to diffusion tensor imaging. NeuroImage 20, 870–888 (2003).

Figures

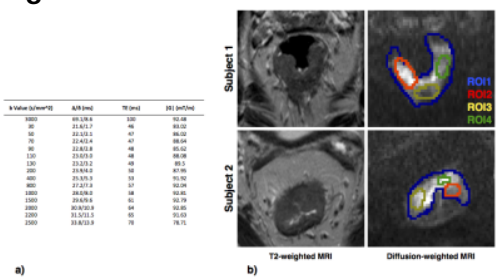

Figure 1: a) shows the DW-MRI acquisition parameters. One non diffusion-weighted acquisition (b=0) and three orthogonal gradient orientations were sampled for each echo time (TE). The repetition time (TR=3588ms) was the same for all acquisitions. b) shows some example data acquired for the two subjects and the ROIs used in the analysis.

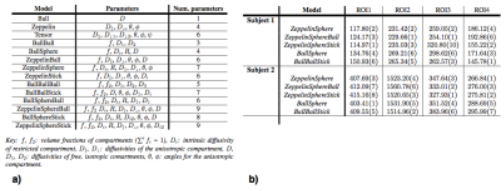

Model	Parameters	Num. parameters
Ball	D	1
Zeppelin	$D_\parallel, D_\perp, \theta, \phi$	4
Tensor	$D_\parallel, D_{\perp_1}, D_{\perp_2}, \theta, \phi, \psi$	6
BallBall	f, D_1, D_2	3
BallSphere	f, D_1, R, D	4
ZeppelinBall	$f, D_\parallel, D_\perp, \theta, \phi, D$	6
ZeppelinSphere	$f, D_\parallel, R, D_\perp, D_\perp, \theta, \phi$	7
ZeppelinStick	$f, D_\parallel, D_\perp, \theta, \phi, D_s$	6
BallBallBall	f, f_2, D_1, D_2, D_3	5
BallBallStick	$f, f_2, D, \theta, \phi, D_s, D_i$	7
BallSphereBall	f, f_2, D_1, R, D_2, D_3	6
ZeppelinSphereBall	$f, f_2, D_\parallel, R, D_\perp, D_\perp, \theta, \phi, D$	9
BallSphereStick	$f, f_2, D_1, R, D_2, \theta, \phi, D$	8
ZeppelinSphereStick	$f, f_2, D_\parallel, R, D_\perp, D_\perp, \theta, \phi, D_2$	9

Key: f, f_2: volume fractions of compartments ($\sum f_i = 1$), D_i: intrinsic diffusivity of restricted compartment, $D_\parallel$, $D_\perp$: diffusivities of the anisotropic compartment, D, D_1, D_2: diffusivities of free, isotropic compartments, θ, ϕ: angles for the anisotropic compartment.

a)

	Model	ROI1	ROI2	ROI3	ROI4
Subject 1	ZeppelinSphere	117.80(2)	231.42(2)	259.05(2)	196.12(4)
	ZeppelinSphereBall	124.17(3)	229.66(1)	254.1(1)	192.86(6)
	ZeppelinSphereStick	114.97(1)	233.03(3)	323.86(10)	155.22(2)
	BallSphere	134.76(4)	269.21(8)	298.62(6)	171.64(3)
	BallBallStick	150.83(6)	265.34(5)	262.57(2)	145.78(1)
Subject 2	ZeppelinSphere	407.69(3)	1525.20(4)	347.64(3)	266.84(1)
	ZeppelinSphereBall	413.08(7)	1560.78(6)	333.01(2)	276.04(3)
	ZeppelinSphereStick	415.16(8)	1520.69(3)	327.93(1)	275.81(2)
	BallSphere	459.41(5)	1531.90(5)	351.32(4)	288.68(5)
	BallBallStick	459.55(5)	1514.96(2)	382.96(6)	295.98(7)

b)

Figure 2: a) lists the models used in the model comparison, which are combinations of the various compartments, as explained in the text. b) show the BIC values of the five best models for each ROI analysed for the subjects. The model rankings for each ROI are shown in brackets (the lower the BIC the higher the model ranking). The list is ordered according to the overall lowest BIC scores for the model in all ROIs of both subjects.

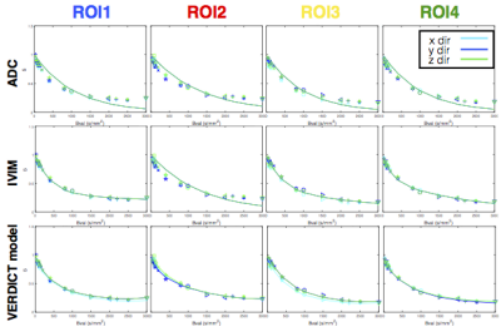

	Model	f	$D_\parallel$	R	f_2	$D_\parallel/D_\perp$	$D_\perp$	D	$f(x)$
ROI1	ZeppelinSphereStick	0.68	2.80	19.0	0.12	12.0	5.96	0.09	−39.06
ROI2	ZeppelinSphereBall	0.24	0.24	4.86	0.23	9.42	3.22	0.92	−96.41
ROI3	ZeppelinSphereBall	0.23	0.49	6.81	0.09	11.8	0.47	1.76	−108.63
ROI4	BallBallStick	0.17	0.05	–	0.17	10.2	–	1.22	−58.56

Diffusivities reported in $\mu m^2/ms$ and R in μm. $f(x)$ denotes the quality of fit.

Figure 3: Synthesised data (lines) for the ADC, IVIM and the VERDICT model, the latter providing the best fit for the ROIs for subject 1. The plots are shown against the effective b-values and different colours denote gradient orientation acquired. The estimated model parameters for the VERDICT models are also shown (symbols explained in Figure.1b). For each ROI, the VERDICT model shown is the one that provides the best fit for the data.

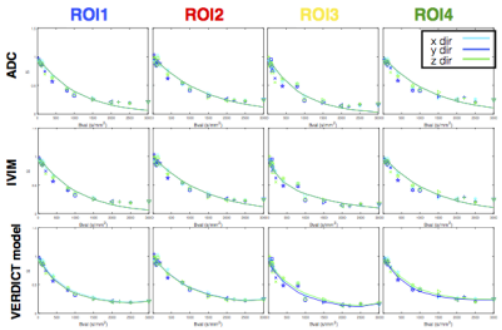

	Model	f	$D_\parallel$	R	f_2	$D_\parallel/D_\perp$	$D_\perp$	D	$f(x)$
ROI1	ZeppelinSphereBall	0.24	0.64	3.74	0.09	2.85	1.90	1.47	−187.62
ROI2	ZeppelinSphereStick	0.06	2.99	19.9	0.76	1.40	1.28	0.61	−741.90
ROI3	ZeppelinSphereStick	0.49	2.71	10.4	0.47	1.59	1.53	11.8	−145.54
ROI4	ZeppelinSphere	0.24	0.42	3.12	0.76	1.65	1.39	–	−119.09

Diffusivities reported in $\mu m^2/ms$ and the R in μm. $f(x)$ denotes the quality of fit.

Figure 4: As Figure.3 but for Subject 2.

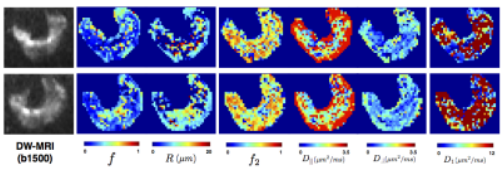

Figure 5: Parameter maps for the ZeppelinSphereBall model, which is one of the best-ranked models for both the subjects. The maps are shown for multiple slices of the dataset for subject 1. The corresponding DW-MRI images are shown for reference. The maps of estimated parameters show: second and third columns - volume fractions and radii for the spherical component, fourth, fifth and sixth columns - volume fraction, parallel diffusivity and perpendicular diffusivity for the anisotropic diffusion component, seventh column – diffusivity of the fast-diffusion component. Note that these maps are produced by fitting a model that assumes an isotropic fast-diffusion compartment.